JASA ARTICLE

Sound power of vibrating cylinders using the radiation resistance matrix and a laser vibrometer

Caleb B. Goates,[1,a)] Cameron B. Jones,[2] Scott D. Sommerfeldt,[1,b)] and Jonathan D. Blotter[2]
[1]*Department of Physics and Astronomy, Brigham Young University, Provo, Utah 84602, USA*
[2]*Department of Mechanical Engineering, Brigham Young University, Provo, Utah 84602, USA*

ABSTRACT:
Research has shown that using acoustic radiation modes combined with surface velocity measurements provide an accurate method of measuring the radiated sound power from vibrating plates. This paper investigates the extension of this method to acoustically radiating cylindrical structures. The mathematical formulations of the radiation resistance matrix and the accompanying acoustic radiation modes of a baffled cylinder are developed. Computational sound power calculations using the vibration-based radiation mode (VBRM) method and the boundary element method are then compared and shown to have good agreement. Experimental surface velocity measurements of a cylinder are taken using a scanning laser Doppler vibrometer and the VBRM method is used to calculate sound power. The results are compared to sound power measurements taken using ISO 3741.
 https://doi.org/10.1121/10.0002870
(Received 4 May 2020; revised 11 November 2020; accepted 12 November 2020; published online 10 December 2020)
[Editor: Li Cheng] Pages: 3553–3561

I. INTRODUCTION

Many methods exist for measuring sound power. The International Organization for Standardization (ISO) has published ten standards and two technical specifications detailing how to obtain sound power measurements. None of the standardized methods are based on vibration measurements and the two technical specifications give only engineering or survey grade results; there is not a precision grade vibration-based method. In the early 1990s, a theory was developed for a method which could potentially fill this void; this method calculates sound power based on a combination of measured surface velocities and acoustic radiation modes.[1]

Acoustic radiation modes provide a convenient basis with which to describe sound radiation from a structure. Structural vibration modes describe the displacement of a structure and satisfy the structural equations of motion and boundary conditions. Conversely, acoustic radiation modes describe the acoustic field; these modes are orthogonal with respect to sound radiation and allow the surrounding acoustical field to be calculated based on the vibrations of a structure. Acoustic radiation modes can be derived from the radiation resistance matrix. The radiation resistance matrix $\mathbf{R}$ relates the normal surface velocities from discrete elements of the structure to the radiated sound power Π of the structure through the equation

$$\Pi(\omega) = \boldsymbol{u}^{\mathrm{H}}(\omega)\mathbf{R}(\omega)\boldsymbol{u}(\omega), \tag{1}$$

where $\boldsymbol{u}$ is a column vector containing the normal velocity at each discrete element, $(\cdot)^H$ signifies the Hermitian transpose, and ω is the frequency of interest.[2] The dependence of various quantities on ω is implied in expressions throughout the remainder of this paper and the (ω) will be omitted. The eigenvectors of the radiation resistance matrix are the acoustic radiation modes, and the corresponding eigenvalues are proportional to the radiation efficiencies of the eigenvectors. The sound power can be written in terms of the acoustic radiation modes $\boldsymbol{q}_r$ and eigenvalues λ_r as

$$\Pi = \sum_{r=1}^{N} \lambda_r |\tilde{y}_r|^2, \tag{2}$$

where $\tilde{y}_r = \boldsymbol{q}_r \cdot \boldsymbol{u}$ and N is the number of elementary radiators over the surface of the structure.[2]

Though the theory behind this approach to calculating sound power has been present for decades, experimental validations did not come until more recently. In 2002, Bai *et al.* published the first experimental sound power calculations based on acoustic radiation modes.[3] Their work showed sound power calculations on baffled flat plates using the most efficiently radiating modes at low frequencies and a modified approach at higher frequencies. The paper showed good agreement between Bai's method and standardized sound power measurements at low frequencies, but the results diverged at higher frequencies. More recent research[4] has shown that acoustic radiation modes can be used to calculate the individual contributions to sound power from multiple uncorrelated sources in a system without having to isolate the sources individually. That research used the vibration-based radiation mode (VBRM) method, which will be used throughout this

[a)]Electronic mail: calebgoates@gmail.com, ORCID: 0000-0001-5745-9902.
[b)]ORCID: 0000-0001-8783-5243.

paper. The VBRM method consists of using complex-valued surface velocity measurements with the radiation resistance matrix to compute the sound power.

In addition to sound power calculations, radiation modes have found use in the field of active structural acoustic control (ASAC).[1,5,6] They have been used for power calculations in computational experiments since they were first introduced. For example, numerical simulations on effectiveness of ASAC control parameters has relied on the radiation modes for evaluation of sound power.[7] Radiation modes have also been used as a guide for structural design, where certain efficient radiation vibration patterns are suppressed through structural modifications.[8] Recent work shows that radiation modes may be used as a basis set for acoustical holography source reconstruction.[9]

Many early papers that develop acoustic radiation modes do so for cylinders. The first three papers that introduced radiation modes included a finite cylinder with hemispherical endcaps[10] and two finite cylinders with flat endcaps.[11,12] In each of these cases, only the axisymmetric modes were calculated. These modes were found by an unspecified numerical method, boundary integral methods, and the boundary element method (BEM), respectively. In addition, at least one other paper has treated the hemispherically capped finite cylinder.[13] Through all these publications there has never been a full development of the radiation modes for a cylinder such that the sound power could be calculated. Boundary element methods or boundary integral equations can be used to calculate the radiation resistance matrix,[9] but an analytical formulation is desirable, as it has the potential to reduce complexity and computational load. More recently, Aslani *et al.*[14] published a formulation for radiation modes of a finite cylinder sandwiched between two infinite pressure release planes using eigenfunction expansion. That formulation limited the radiation to a space that extended only from 0 to L in the z dimension. This paper will follow and expand upon the formulation of Aslani *et al.* to develop a full analytical expression for the radiation resistance matrix of vibrating cylinders with infinite cylindrical baffles radiating into a full three-dimensional space. This cylindrical radiation resistance matrix will be used to calculate sound power of cylindrical objects in both computational and experimental settings. While there are cylindrical structures in engineering applications, we recognize that most structures to which it would be desirable to apply this method will not be cylindrical, and even fewer will be infinitely baffled. The results presented herein show that it may not be necessary to have such exact matching between the experimental acoustic environment and the environment used for deriving the radiation resistance matrix. The formulations derived in this paper are a step toward a method of treating more general curved structures.

II. CYLINDER RADIATION MODES

A. Eigenfunction formulation of the radiation resistance matrix

The radiation resistance matrix is derived from the pressure that a small vibrating element of a structure generates across the structure. This small vibrating element can be treated mathematically as a point source, or as a small rectangular element with constant velocity. We choose to use the latter, as it more closely matches the discretization that will be used later in the paper. It is worth noting that a delta function could be used in the following derivations to represent the velocity with an identical derivation result. As shown in Fig. 1, assume that a small portion of a hard, infinite cylinder is vibrating with velocity

$$u(\theta,z)=\begin{cases} u_0, & \theta_1\le\theta\le\theta_2,\ z_1\le z\le z_2 \\ 0, & \text{otherwise} \end{cases} \tag{3}$$

for some θ_1, θ_2 and z_1, z_2 such that $a\Delta\theta\equiv a(\theta_2-\theta_1)\ll 2\pi/k$ and $\Delta z\equiv(z_2-z_1)\ll 2\pi/k$, where k is the acoustic wavenumber and a is the radius of the cylinder. This vibration creates a pressure field that can be written in terms of cylindrical eigenfunctions as

$$p(r,\theta,z)=\sum_{m=0}^{\infty}\int_0^{\infty}dk_z(A_m\cos m\theta+B_m\sin m\theta)\times(E(k_z)\cos k_z z+F(k_z)\sin k_z z)H_m^{(2)}(k_r r), \tag{4}$$

where $k_r=\sqrt{k^2-k_z^2}$, k_z is the axial acoustic wavenumber, m is an integer, $H_m^{(2)}(x)$ is the m th-order Hankel function of the second kind, and A_m, B_m, $E(k_z)$, and $F(k_z)$ are coefficients yet to be determined. For this expression, $e^{j\omega t}$ time dependence has been assumed, where $j=\sqrt{-1}$. The Hankel function of the first kind is omitted as the absence of sources outside $r=a$ precludes incoming cylindrical waves. The coefficients are determined by the surface condition at $r=a$ of

$$\left.\frac{\partial p}{\partial r}\right|_{r=a}=-j\rho_0\omega\,u(\theta,z), \tag{5}$$

where ρ_0 is the density of air and ω is the angular frequency. To apply this boundary condition, the velocity given in

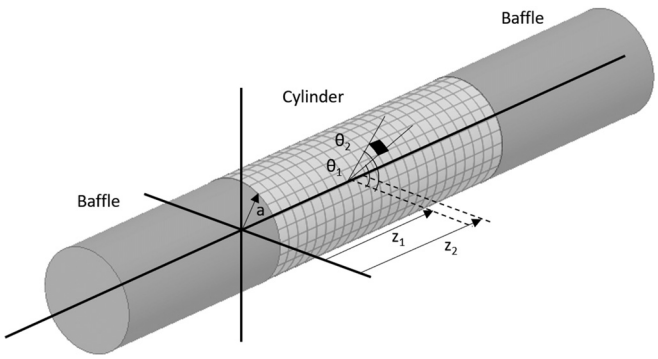

FIG. 1. A diagram of the infinitely baffled cylinder geometry. A discretization of the non-rigid portion of the cylinder is shown, with the element described in Eq. (3) highlighted in black.

https://doi.org/10.1121/10.0002870

Eq. (3) can also be represented in terms of the θ and z cylindrical eigenfunctions as

$$u(\theta,z) = \int_0^\infty dk_z\,(e(k_z)\cos k_z z + f(k_z)\sin k_z z) \times \sum_{m=0}^{\infty}(a_m\cos m\theta + b_m \sin m\theta). \tag{6a}$$

Equation (6a) can be set equal to Eq. (3) to find the coefficients a_m, b_m, $d(k_z)$, and $e(k_z)$. Because Eq. (6a) is a separable expression in θ and z, their dependence may be treated separately,

$$\sum_{m=0}^{\infty}(a_m\cos m\theta + b_m\sin m\theta) = \begin{cases} u_0, & \theta_1 \le \theta \le \theta_2 \\ 0, & \text{otherwise,} \end{cases} \tag{6b}$$

$$\int_0^\infty (e(k_z)\cos k_z z + f(k_z)\sin k_z z)dk_z = \begin{cases} 1, & z_1 \le z \le z_2 \\ 0, & \text{otherwise,} \end{cases} \tag{6c}$$

where the constant u_0 has been arbitrarily assigned to the θ-dependent expression. The coefficients may now be solved for using orthogonality and sine and cosine transforms,

$$\begin{aligned} a_m &= \frac{u_0}{\varepsilon_m\pi}\int_{\theta_1}^{\theta_2}\cos m\theta d\theta \approx \frac{u_0\Delta\theta}{\varepsilon_m\pi}\cos m\theta_0, \\ b_m &= \frac{u_0}{\pi}\int_{\theta_1}^{\theta_2}\sin m\theta d\theta \approx \frac{u_0\Delta\theta}{\pi}\sin m\theta_0, \\ e(k_z) &= \frac{1}{\pi}\int_{z_1}^{z_2}\cos k_z z dz \approx \frac{\Delta z}{\pi}\cos k_z z_0, \\ f(k_z) &= \frac{1}{\pi}\int_{z_1}^{z_2}\sin k_z z dz \approx \frac{\Delta z}{\pi}\sin k_z z_0, \end{aligned} \tag{7}$$

where $z_0 = (z_2+z_1)/2$, $\Delta z = z_2 - z_1$, $\theta_0 = (\theta_2+\theta_1)/2$, $\Delta\theta = \theta_2 - \theta_1$, and

$$\varepsilon_m = \begin{cases} 1, & m \ne 0 \\ 2, & m = 0. \end{cases} \tag{8}$$

The approximate equalities hold because Δz and $a\Delta\theta$ are small compared to the acoustic wavelength. Substituting Eq. (7) into Eq. (6a), applying the boundary conditions in Eq. (5), and simplifying results in the final pressure expression

$$p(r,\theta,z) = -j\frac{u_0\rho_0\omega\Delta\theta\Delta z}{\pi^2}\int_0^\infty \frac{dk_z}{k_r}\cos\left[k_z(z-z_0)\right] \times \sum_{m=0}^{\infty}\frac{H_m^{(2)}(k_r r)}{\varepsilon_m H_m^{(2)'}(k_r a)}\cos\left[m(\theta-\theta_0)\right]. \tag{9}$$

Dividing Eq. (9) by the velocity of the vibrating element, i.e., u_0, and evaluating at a surface element gives the mutual impedance between the source point, point i, and the field point, j, such that

$$Z_{pq} = -j\frac{\rho_0\omega\Delta\theta\Delta z}{\pi^2}\int_0^\infty \frac{dk_z}{k_r}\cos\left[k_z(z_q-z_p)\right] \times \sum_{m=0}^{\infty}\frac{H_m^{(2)}(k_r a)}{\varepsilon_m H_m^{(2)'}(k_r a)}\cos\left[m(\theta_q-\theta_p)\right]. \tag{10}$$

The radiation resistance matrix is concerned only with the real part of this expression. Thus, since $H_m^{(2)}(k_r a)/k_r H_m^{(2)'}(k_r a)$ is purely real for imaginary k_r, the integration need only be carried out from 0 to k. The elements of the radiation resistance matrix are then found as

$$\begin{aligned} R_{pq} &= \frac{S_e}{2}\mathrm{Re}\{Z_{pq}\} \\ &= \frac{S_e^2\omega\rho_0}{a\pi^2}\int_0^k \frac{dk_z}{k_r}\cos\left[k_z(z_q-z_p)\right] \\ &\quad\times \sum_{m=0}^{\infty}\frac{1}{\varepsilon_m}\mathrm{Im}\left\{\frac{H_m^{(2)}(k_r a)}{H_m^{(2)'}(k_r a)}\right\}\cos\left[m(\theta_q-\theta_p)\right], \end{aligned} \tag{11}$$

where $S_e = a\Delta\theta\Delta z$ is the area of a single discrete element of the structure, and the summation has been moved inside the integral.

B. Numerical evaluation

Equation (11) is not closed-form; it involves an infinite sum that must be truncated and an integral that must be numerically evaluated. This section offers guidance on how the expression may be evaluated.

The sum is performed first for each integration point. As m increases from 0, the ratio $\mathrm{Im}\{H_m^{(2)}(k_r a)/H_m^{(2)'}(k_r a)\}$ starts at a value of $\frac{1}{2}$, peaks at $m \approx k_r a$, then monotonically decreases, approaching zero rapidly, as shown in Fig. 2. Therefore, this coefficient is used as the test for convergence. For the purposes of this research, once $\mathrm{Im}\{H_m^{(2)}(k_r a)/H_m^{(2)'}(k_r a)\} < 10^{-8}$, the sum is considered to have converged.

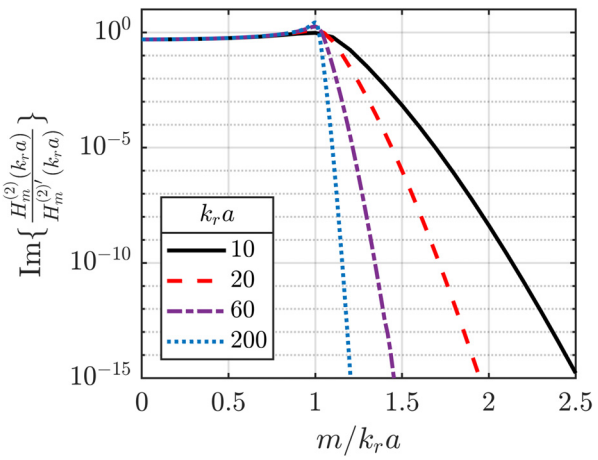

FIG. 2. (Color online) Plot of $Im\{H_m^{(2)}(k_r a)/H_m^{(2)'}(k_r a)\}$ as a function of m, for different values of $k_r a$. In each case, the ratio peaks near $m = k_r a$, then monotonically decreases to zero.

The truncated sums may be calculated at desired integration points as dictated by a given integration method. This paper uses the midpoint rule, with the integrand evaluated at 80 points over the interval $[0, k]$. Though this is a rather simple method to perform the integration, it has been shown to be sufficiently accurate for the purposes of this research.

It appears there could be a singularity in the integral at $k_z = k$, where k_r becomes zero. Use of the limiting forms of the Hankel functions as the argument goes to zero shows that

$$\lim_{k_r \to 0} \mathrm{Im}\left\{H_m^{(2)}(k_r a)/H_m^{(2)'}(k_r a)\right\}/k_r = 0,$$

so the integrand may be replaced with zero at the endpoint if it is needed for the chosen integration method.

C. Radiation modes

Acoustic radiation modes are computed with an eigendecomposition of the radiation resistance matrix[12] and provide a useful way to characterize **R**. The eigenvectors represent the acoustic radiation modes while the associated eigenvalues are proportional to the radiation efficiency. The first nine radiation modes from the formulation above, ordered by the radiation efficiency of the mode, are shown in Fig. 3 for a cylinder with $a/L = 0.2$ at $ka = 0.01$ rad. The first mode resembles a monopole with all parts of the cylinder vibrating in phase and at equal amplitude. The next three modes resemble dipoles and the final five modes resemble quadrupoles. Due to the symmetries associated with a cylinder, all radiation modes with θ dependence come in pairs of degenerate modes.

Figure 4 shows the nine most efficient radiation modes for $ka = 1$. The first four modes follow the same pattern exhibited in Fig. 3, though the amplitude is tapered toward the ends of the cylinder. The fourth mode in Fig. 4 is the second mode from Fig. 3, which has been overtaken by the third and fourth modes from Fig. 3 in efficiency. The eighth and ninth modes in Fig. 4 are new modes which were not seen in Fig. 3.

The modal efficiencies with respect to ka also give insight into the modal behavior. Efficiencies are plotted in Fig. 5 for each of the nine modes shown in Fig. 3, with degenerate mode efficiencies combined into one line. This plot shows the monopole/dipole/quadrupole radiation characteristics of the modes at low ka: The first mode increases in efficiency, and therefore power, at a rate of 6 dB/octave, the next three modes at 12 dB/octave, and the last five at 18 dB/octave. The trends with frequency of these modes and their efficiencies are treated with more detail in a proceedings article by the authors.[15]

Sound power can be calculated using either the radiation resistance matrix as in Eq. (1), or the acoustic radiation modes, as in Eq. (2). Use of the radiation resistance matrix requires a matrix-vector multiplication and a dot product while use of acoustic radiation modes requires an eigenvalue

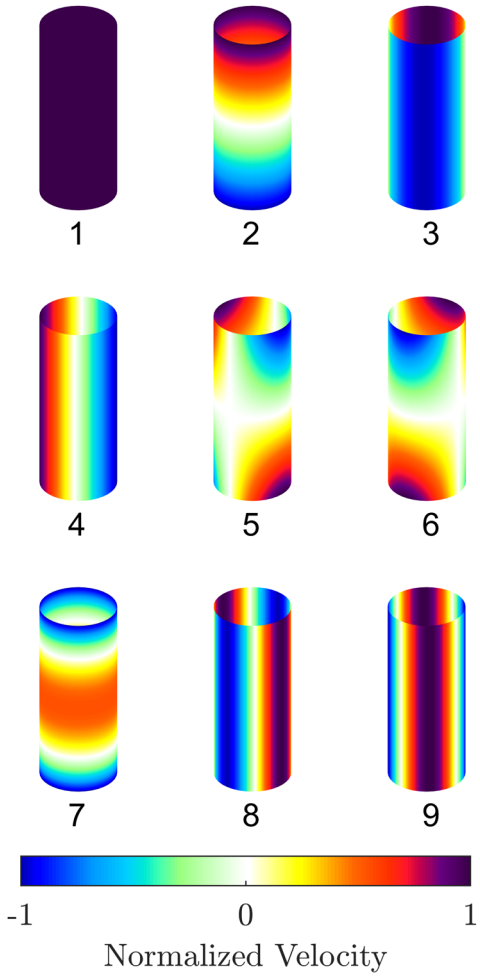

FIG. 3. (Color online) The nine most efficient radiation modes for a baffled cylinder with $a/L = 0.2$ and $ka = 0.01$.

decomposition of a matrix, several dot products to find $\tilde{y}_r$, and a sum. Since the complexity of eigenvalue decomposition is theoretically limited to that of matrix-vector multiplication[16,17] and is in practice much slower, there is no benefit to using the acoustic radiation modes for the sound power calculation presented in this work. It is possible that interpolation of the radiation modes could, in some future work, make radiation modes faster for power computation, but in the simple uses described by Eqs. (1) and (2) there is no real benefit to using the radiation modes. We therefore expand the acronym VBRM to include vibration-based radiation resistance matrix. The VBRM method power curves in this paper are calculated using the radiation resistance matrix given in Eq. (11) as demonstrated in Eq. (1). For brevity, the cylindrical radiation resistance matrix will not be explicitly mentioned in Secs. III and IV; however, the following validations treat both the method and the resistance matrix.

III. COMPUTATIONAL VERIFICATION OF SOUND POWER CALCULATIONS

To verify the methodology above, sound power calculations performed using the VBRM method as just described

https://doi.org/10.1121/10.0002870

were compared to those performed with the boundary element method (BEM). BEM simulations were performed using VibroAcoustics One (VA One), a commercial package produced by the ESI Group. The comparison was conducted on a 41 cm long cylinder with a 7.6 cm radius. The infinite cylindrical baffle assumed in the theory was approximated in the BEM simulations by a 1-meter baffle connected to each end of the vibrating portion of the cylinder. Simulations were also performed with rigid ends on the cylinder instead of a baffle, and these results showed that the baffle had a negligible effect on the radiated sound power. The VA One simulation used linear tri elements, while the VBRM method as formulated above is effectively using constant quad elements. As such, the integration of the sound power in the VBRM method is performed by multiplying velocity values at the center of each element by the element area. This is handled automatically by the expression in Eq. (11).

Once the cylinder was modeled in VA One, the surface velocities of the shell were computed at each nodal point of the VA One mesh and at the center of each VBRM element using the modal expansion method developed by Bernoulli for a cylinder excited by a point force.[18] The complex normal surface velocities were calculated as

$$u_3(x,\theta) = \frac{2P}{\rho h a L \pi} \sum_{m=1}^{\infty} \sum_{n=0}^{\infty} \frac{\sin(m\pi z^*/L)\sin(m\pi z/L)\cos n(\theta-\theta^*)}{\varepsilon_n \omega_{mn}^2 \sqrt{\left[1-(\omega/\omega_{mn})^2\right]^2 + 4\zeta_{mn}^2(\omega/\omega_{mn})^2}} e^{-j\phi_{mn}}, \tag{12}$$

where P is the point load, ρ is the density of the cylinder's material, h is the thickness of the cylindrical wall, L is the length of the cylinder, m and n are the longitudinal and radial mode numbers, respectively, z^* and θ^* are the longitudinal and radial location of the point force, z and θ are the longitudinal and radial locations of the nodal points, ω is the angular frequency of interest, ω_{mn} is the natural angular frequency of a given mode, ζ_{mn} is the damping coefficient of each mode,

$$\phi_{mn} = \tan^{-1}\frac{2\zeta_{mn}(\omega/\omega_{mn})}{1-(\omega/\omega_{mn})^2}, \tag{13}$$

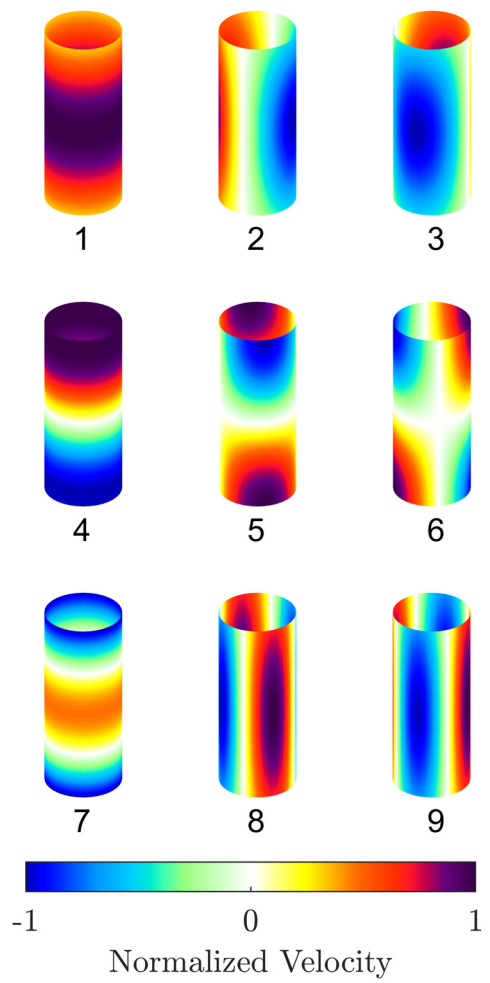

FIG. 4. (Color online) The nine most efficient radiation modes for a baffled cylinder with $a/L = 0.2$ and $ka = 1$.

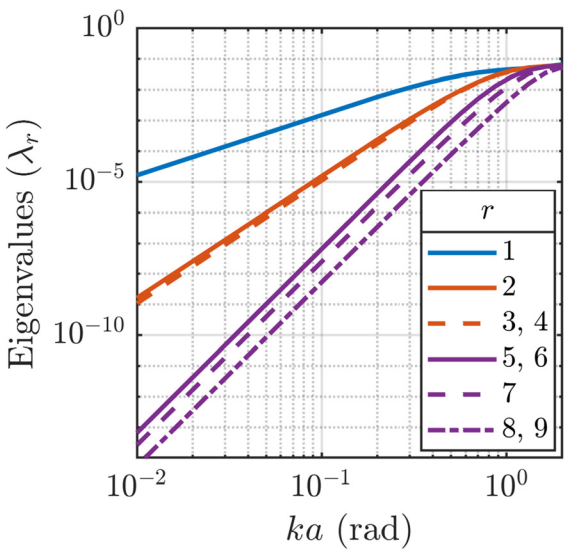

FIG. 5. (Color online) Efficiencies of the nine radiation modes that are most efficient at low ka. Degenerate mode efficiencies are combined into one line.

and ε_n is defined as in Eq. (8). The infinite series in Eq. (12) were truncated at $m = 19$, $n = 19$, and a damping coefficient of $\zeta_{mn} = 0.1$ for each m, n was used in the calculation. These velocities were supplied to the VA One BEM simulation and to the VBRM method, which were then used to calculate the sound power of the cylinder.

Multiple simulations were performed using the VBRM method with different spatial sampling grids and different numbers of elements to analyze the effect of the spatial sampling. Velocities were calculated with the following spatial sampling patterns (longitudinal elements × theta elements): 8×9 (72 elements), 10×12 (120 elements), 16×19 (304 elements), and 26×31 (804 elements). Figure 6 shows the computational results using the VBRM method for each of these grids. The 72-element spatial sampling simulation agrees with simulations using a denser spatial sampling below 1.5 kHz. Above 1.5 kHz the results begin to diverge. The 120-element spatial sampling simulation agrees with simulations using a denser spatial sample until 3 kHz, after which the results diverge. The reason for the divergence of the 72- and 120-element simulations is due to the low spatial sampling density associated with fewer data points. The 304-element simulation and the 806-element simulation agree exactly throughout the 6 kHz range shown on the plot.

The sound power results from the 304-element simulation shown in Fig. 6 were compared with the sound power results calculated using the BEM method for validation of the VBRM method. The BEM mesh was constructed to contain at least 6 elements per wavelength in the frequency range of interest and contained 1121 elements and 1157 degrees of freedom. These results are shown in Fig. 7, with the two methods giving nearly identical results at most frequencies. The VBRM method calculates sound power to be slightly higher between 3 and 4 kHz but the difference between the two methods is less than 1.5 dB at each frequency.

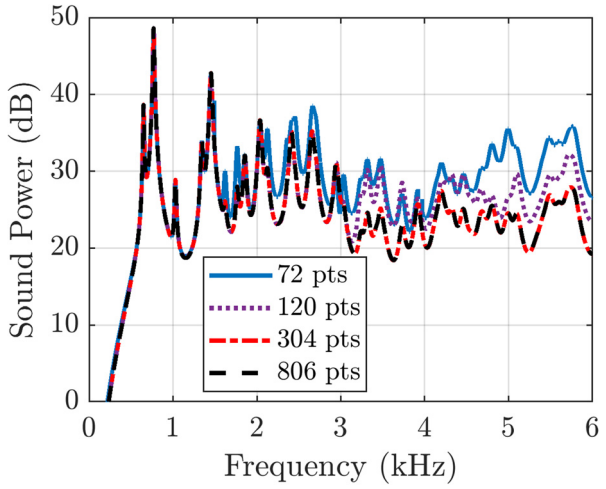

FIG. 6. (Color online) Numerically calculated sound power using the radiation resistance matrix and simulated complex velocities at several different numbers of data points.

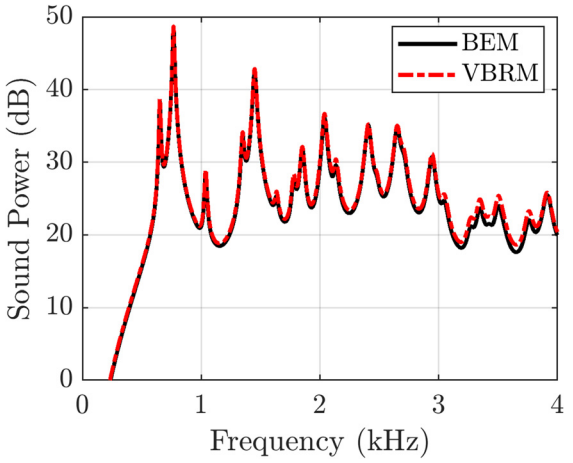

FIG. 7. (Color online) Numerically derived sound power of a 41 cm long cylinder with a 7.6 cm radius using the VBRM and BEM methods.

The VBRM method and BEM method were also used to calculate the sound power of a 41 cm long cylinder with a 15.2 cm radius. Due to the larger surface area of the 15.2 cm radius cylinder, the number of elements used in the VBRM simulation was increased to 576 to ensure the spatial sampling was dense enough for accurate results. The number of elements in the BEM mesh was also increased to 2256 elements, with 2330 degrees of freedom. Figure 8 shows the comparison between the two methods for this cylinder. Like the results from the 7.6 cm radius cylinder, the results from the two methods for the 15.2 cm radius cylinder line up at most frequencies, with slight discrepancies at frequencies higher than 3 kHz. These discrepancies are less than 1.5 dB.

Because constructing a rigid baffle for experimental tests is difficult, additional BEM simulations were run to determine how sensitive sound power calculations are to the presence of a baffle. The BEM calculations in Fig. 7 were repeated with the same mesh on the cylinder and the same cylinder velocities, but with rigid end caps instead of a rigid baffle. The results, shown in Fig. 9, are less than 1 dB apart above 90 Hz, and are less than 0.2 dB above 470 Hz.

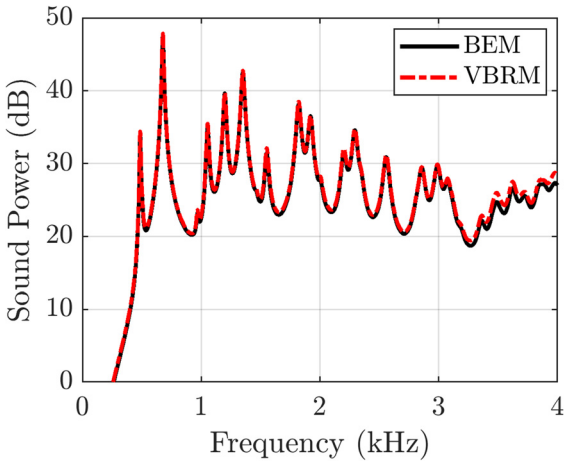

FIG. 8. (Color online) Numerically derived sound power of a 41 cm long cylinder with a 15.2 cm radius using the VBRM and BEM methods.

https://doi.org/10.1121/10.0002870

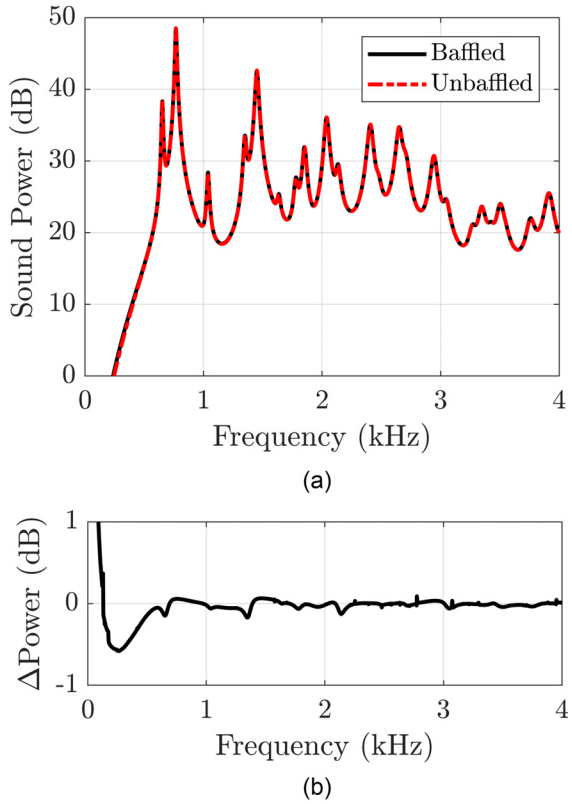

FIG. 9. (Color online) Numerical comparison between a baffled and an unbaffled 41 cm long cylinder with a 7.6 cm radius using the BEM method. (a) The sound power of the baffled and unbaffled cylinders. (b) The difference in sound power between the baffled and unbaffled cylinders.

This suggests that sound power calculations may not be sensitive to the presence of a baffle.

IV. EXPERIMENTAL VERIFICATION OF SOUND POWER CALCULATIONS

This section will detail the experimental sound power measurement of a cylinder using the VBRM method. The results calculated using the VBRM method will then be compared to sound power measurements taken using ISO 3741 in a large reverberation chamber, with the results being reported in one-third octave bands. While the formulation presented above treats a cylinder with an infinite rigid baffle, our experimental measurements and the numerical results above suggest that the exact matching of that acoustic boundary condition is not necessary to get accuracy rivaling that of sound power measurement standards. In other words, the results below suggest that radiation resistance matrices need not exactly match the acoustic environment to get accurate sounds power measurements.

A. Experimental setup and measurement of a cylindrical shell

A 41 cm long aluminum cylinder with a radius of 7.6 cm and flat endcaps was mounted on a plywood board as shown in Fig. 10. A Modal Shop 2007E shaker was supported by the same plywood board with a small piece of foam minimizing the transfer of vibrations from the shaker to the plywood. The stinger of the shaker was attached to the cylinder 8.5 cm from its bottom edge. The mounted cylinder and shaker were then attached to an Outline ET250-3D electronic turntable and placed in a reverberation chamber with approximate dimensions 5 m × 6 m × 7 m. In preparation to make ISO 3741 sound power measurements, six microphones were set up inside the reverberation chamber according to guidelines of the standard.

FIG. 10. (Color online) Setup of a mounted cylinder on a turntable with a shaker to excite the cylinder. The microphones and reverberation chamber used for ISO 3741 are seen in the background.

The experimental setup described above does not perfectly match the theoretical and computational assumptions presented in previous sections. Sections II and III assumed an infinite cylindrical baffle (approximated by a 1-m baffle in VA One) extending from each end of the cylinder, and simulations treated a simply supported cylinder. While the radiation resistance matrix is independent of structural boundary conditions, the lack of a cylindrical baffle and the presence of a turntable and wooden base are departures from assumptions made in the preceding formulations. Because of the BEM results presented already comparing a baffled and unbaffled cylinder (see Fig. 9), those departures are not expected to significantly alter the results.

The shaker was excited using pseudo-random noise between 0 and 12.4 kHz. Using a scanning laser Doppler vibrometer (SLDV), line scans measuring the complex surface velocities of the cylinder were taken at 10° intervals around the circumference of the cylinder. Each line scan contained 31-points, resulting in a total of 1116 scan points over the surface of the cylinder. This number of experimental points was well above the number of points needed to obtain accurate results up to 6 kHz, as shown in Fig. 6. Figure 11 shows an example of one line scan.

The shaker blocked a small section of the cylinder from the laser, making surface velocity measurements in that area

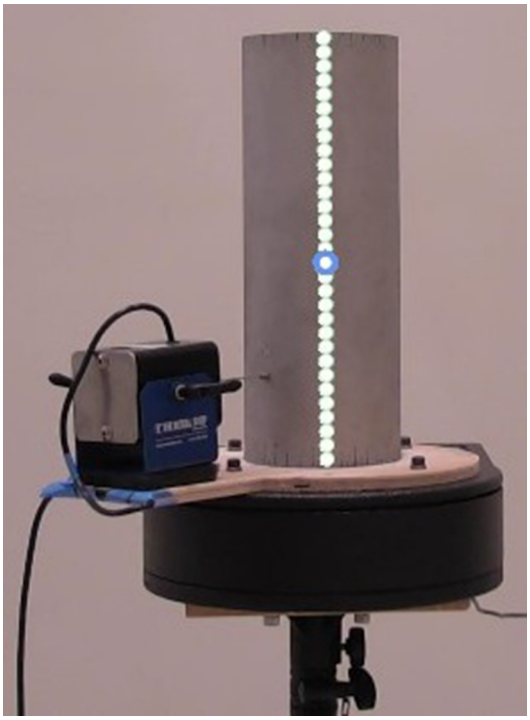

FIG. 11. (Color online) Example of one of the 36 line scans taken over the surface of the cylinder to measure complex surface velocities.

unobtainable. As such, velocity data from points 180° from the blocked points were used to approximate these velocity data, at a total of 25 out of the 1116 scan points. Due to the proximity of the blocked portions of the cylinder to the point of excitation, the approximated velocity data at those points are likely underestimations. These approximate velocity data, along with measured data at the other locations, were then used as inputs to the VBRM method.

After the surface velocity measurements were collected, the SLDV was removed from the reverberation chamber, and sound pressure measurements were taken according to the procedures set forth in ISO 3741. Sound power was calculated according to ISO 3741, and the calculated sound power measurements using the VBRM method were then compared to these standard results, reported in one-third octave bands.

B. Sound power results of the cylinder

Figure 12 shows the comparison between the VBRM method and the ISO 3741 sound power results. The results are also summarized in Table I which shows the difference between the methods at each one-third octave band. Below 200 Hz the ISO measured sound power results were within 10 dB of the noise floor of the chamber; the results at these frequencies should therefore be considered upper bounds on the radiated sound power. Between the 200 Hz and 10 kHz one-third octave bands there is good alignment between the two methods: In this region the mean difference between the two methods was 0.3 dB with a standard deviation of 1.6 dB. The maximum one-third octave band difference was 2.1 dB

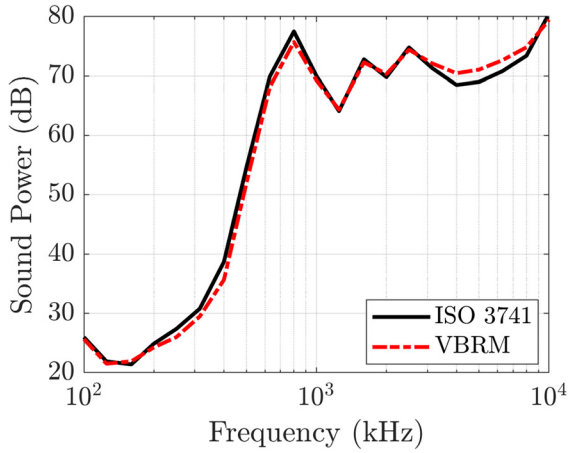

FIG. 12. (Color online) Results of the sound power measurements using the VBRM method compared to the ISO 3741 standard results.

at the 5 kHz band. These experimental differences are in line with the differences seen between the BEM and VBRM methods compared in Figs. 7 and 8. In addition, the overall levels are very close, as seen in Table I, with only 0.4 dB difference between the two methods.

The differences between the two methods could be the result of the experimental setup. The theoretical and computational work assumed an infinitely baffled cylinder, but the experimental setup included endcaps on each end of the cylinder instead of a baffle. While computational experiments showed no difference between a baffled cylinder and a cylinder with rigid endcaps, the endcaps in the physical

TABLE I. Results of the sound power measurements using ISO 3741 and the VBRM method, and the difference between the two.

		Sound power (dB)		
		ISO 3741	VBRM	Difference
Third octave band by centerband frequency (Hz)	100	26.0	25.7	0.3
	125	21.9	21.5	0.4
	160	21.4	21.9	(0.5)
	200	24.9	24.3	0.6
	250	27.4	26.0	1.4
	315	30.8	29.5	1.3
	400	38.7	35.7	3.0
	500	54.6	52.0	2.6
	630	69.9	68.1	1.8
	800	77.5	75.7	1.8
	1000	70.0	69.3	0.7
	1250	64.1	64.3	(0.3)
	1600	72.8	72.3	0.5
	2000	69.8	70.3	(0.5)
	2500	74.8	74.4	0.4
	3150	71.3	72.1	(0.8)
	4000	68.5	70.4	(2.0)
	5000	69.0	71.1	(2.1)
	6300	70.8	72.6	(1.9)
	8000	73.4	74.8	(1.4)
	10 000	80.5	79.5	1.0
	Total	84.9	84.6	0.4

https://doi.org/10.1121/10.0002870

cylinder were not rigid, and therefore may have radiated noise which contributed to the sound power measured by ISO 3741. The experimental setup of the cylinder also included a plywood mount, a turntable, and a shaker, each of which could have vibrated from contact with the cylinder. These surfaces were not measured using the SLDV, thus any contribution they made to sound power would be measured by ISO 3741 but not by the VBRM method.

V. CONCLUSIONS

After a brief review of the concept of radiation resistance matrices and their uses, a derivation of the cylindrical radiation resistance matrix was presented. This produced a full, analytical expression for the matrix, which can be used in sound power calculations. The radiation modes computed from this matrix were shown to match multipole trends at low frequencies, as would be expected from canonical radiation modes for other geometries. Numerical methods to evaluate the non-closed form equations were presented.

Following the derivation of the cylindrical radiation resistance matrix, sound power was computed for analytical simply supported shell velocities using the VBRM method with this matrix. This power was compared to that calculated by BEM, which is treated as a benchmark. These results showed very good agreement between 0 Hz and 4 kHz with discrepancies of less than 1.5 dB appearing in some higher frequency bands.

Experimental surface velocity measurements of an unbaffled cylinder were collected using an SLDV and the sound power was determined using the VBRM method and the cylindrical radiation resistance matrix. The sound power was also measured using ISO 3741. These experimental results showed good agreement through the 10 kHz one-third-octave band. Between the 200 Hz and 10 kHz one-third octave bands the mean difference in the sound power obtained using ISO 3741 and the VBRM method was 0.3 dB with a standard deviation of 1.6 dB. The maximum difference between the two methods in any one-third octave band was 2.1 dB which occurred at the 5 kHz one-third octave band.

The results of the numerical simulations and the experimental work presented in this paper have shown that the cylindrical radiation resistance matrix developed in the paper, implemented into the VBRM method, allows for the sound power measurement of baffled cylinders. In addition, the results presented here indicate that a radiation resistance matrix developed for cylinders with infinite cylindrical baffles may accurately compute power for finite unbaffled cylinders, and that an exact match of the radiation resistance matrix to the acoustic conditions may not be required.

[1]S. J. Elliot and M. E. Johnson, "Radiation modes and the active control of sound power," J. Acoust. Soc. Am. **94**(4) 2194–2204 (1993).
[2]F. Fahy and P. Gardonio, "Sound radiation by vibrating structures," in *Sound and Structural Vibration*, in *Radiation, Transmission and Response*, 2nd ed. (Academic Press, Oxford, UK, 2007).
[3]M. R. Bai and M. Tsao, "Estimation of sound power of baffled planar sources using radiation matrices," J. Acoust. Soc. Am. **112**, 876–883 (2002).
[4]C. B. Jones, C. B. Goates, J. D. Blotter, and S. D Sommerfeldt, "Experimental validation of determining sound power measurements using acoustic radiation modes and a laser vibrometer," Appl. Acoust. **164**, 107254 (2020).
[5]Y. Cao, S. D. Sommerfeldt, W. Johnson, J. D. Blotter, and P. Aslani, "An analysis of control using the weighted sum of spatial gradients in active structural acoustic control for flat panels," J. Acoust. Soc. Am. **138**, 2986–2997 (2015).
[6]P. Aslani, S. D. Sommerfeldt, and J. D. Blotter, "Experimental active control of cylindrical shells using the weighted sum of spatial gradients control metric," J. Acoust. Soc. Am. **143**, 271–280 (2018).
[7]J. M. Fisher, J. D. Blotter, S. D. Sommerfeldt, and K. L. Gee, "Development of a pseudouniform structural quantity for use in active structural acoustic control of simply supported plates: An analytical comparison," J. Acoust. Soc. Am. **131**, 3833–3840 (2012).
[8]J. Liu, Y. Liu, and J. S. Bolton, "The application of acoustic radiation modes to engine oil pan design," SAE Technical Paper No. 2017-01-1844 (2017).
[9]J. Liu, Y. Liu, and J. S. Bolton, "Acoustic source reconstruction and visualization based on acoustic radiation modes," J. Sound Vib. **437**, 358–372 (2018).
[10]D. M. Photiadis, "The relationship of singular value decomposition to wave-vector filtering in sound radiation problems," J. Acoust. Soc. Am. **88**(2), 1152–1159 (1990).
[11]G. V. Borgiotti, "The power radiated by a vibrating body in an acoustic fluid and its determination from boundary measurements," J. Acoust. Soc. Am. **88**(4), 1884–1893 (1990).
[12]A. Sarkissian, "Acoustic radiation from finite structures," J. Acoust. Soc. Am. **90**(1), 574–578 (1991).
[13]G. V. Borgiotti and K. E. Jones, "Frequency independence property of radiation spatial filters," J. Acoust. Soc. Am. **96**(6), 3516–3524 (1994).
[14]P. Aslani, S. D. Sommerfeldt, and J. D. Blotter, "Analysis of external radiation from circular cylindrical shells," J. Sound Vib. **408**, 154–167 (2017).
[15]C. B. Goates, S. D. Sommerfeldt, and J. D. Blotter, "Frequency trends of acoustic radiation modes for cylindrical structures," Proc. Mtgs. Acoust. **35**, 065003 (2018).
[16]J. Demmel, I. Dumitriu, and O. Holtz, "Fast linear algebra is stable," Numer. Math. **108**(1) 59–91 (2007).
[17]S. Winograd, "On the number of multiplications necessary to compute certain functions," Commun. Pure Appl. Math. **23**(2), 165–179 (1970).
[18]W. Soedel, *Vibrations of Shells and Plates*, 2nd ed., *revised and expanded* (Marcel Dekker, New York, 1993).